Self-Doped Rutile Titania with High Performance for Direct and Ultrafast Assay of H$_2$O$_2$

Shu Sheng Pan,*[†,‡] Wei Lu,[†] Yi Hua Zhao,[§] Wei Tong,[⊥] Ming Li,[‡] Li Min Jin,[†] Jin Yuk Choi,[†] Fei Qi,[#] Shi Guo Chen,[∥] Lin Feng Fei,[†] and Siu Fung Yu*[†]

[†]Department of Applied Physics, [#]Department of Civil and Environmental Engineering, and [∥]Department of Applied Biology and Chemical Technology, The Hong Kong Polytechnic University, Hung Hom, Kowloon, Hong Kong, China

[‡]Key Laboratory of Materials Physics, Anhui Key Laboratory of Nanomaterials and Nanostructures, Institute of Solid State Physics, and [⊥]Steady High Magnetic Field Facility, High Magnetic Field Laboratory, Chinese Academy of Sciences, Hefei 230031, Anhui, People's Republic of China

[§]Department of Chemistry, Hong Kong University of Science and Technology, Clear Water Bay, Kowloon, Hong Kong, China

Ⓢ Supporting Information

ABSTRACT: Detection of H$_2$O$_2$ is important for the applications in environmental protection, pharmaceutical industries, food production, and clinical control. Current colorimetric assay of H$_2$O$_2$ based on enzyme or nanomaterials always needs TMB or other peroxidase substrate as coloration species. Furthermore, the corresponding response time including incubation process is in order of minute. In this study, we report on the synthesis of heavily Ti^{3+}-doped TiO$_2$ composed of spherelike nanoparticles by pulsed laser ablation method. This TiO$_2$ can directly detect H$_2$O$_2$ without using TMB or any other peroxidase substrate and is free from incubation process. In addition, the detection sensitivity is compatible with or better than that of the natural enzyme or other nanomaterials. Hence, the self-doped TiO$_2$ nanoparticles provide a novel, direct, ultrafast approach for H$_2$O$_2$ assay application.

KEYWORDS: H$_2$O$_2$ assay, Ti^{3+} self-doping, titanium oxide, absorption, nanotechnology
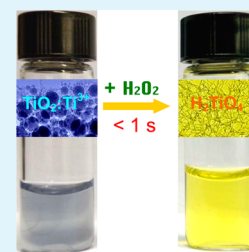
1. INTRODUCTION

Hydrogen peroxide (H$_2$O$_2$) is an indispensable intermediate product in most of the environmental and biological circulation processes so that rapid and accurate detection of H$_2$O$_2$ is essential for environmental protection pharmaceutical industries, food production, and clinical control.[1,2] Therefore, the development of rapid, efficient and sensitive methodologies for H$_2$O$_2$ detection is of great interest and extensive attention has been concentrated on the realization of novel H$_2$O$_2$ assay. Horseradish peroxidase (HRP), which is a natural enzyme, has been utilized to assay H$_2$O$_2$. This is because HRP is sensitive to the presence of H$_2$O$_2$ and selectively in catalyzing H$_2$O$_2$ reduction in biological solutions.[3] However, the reaction time of enzymes with H$_2$O$_2$ is usually very long (i.e., in tens of minutes) and the preparation/purification cost of enzymes is expensive. In addition, enzymes may malfunction in harsh environment and tend to denature under normal detection conditions. Hence, despite the high detection sensitivity of HRP, artificial enzyme mimics were developed to replace natural enzymes for the assay of H$_2$O$_2$.

Up to now, various nanomaterials including iron oxide-based nanocomposite,[1−5] carbon nanotubes,[6] graphene oxide,[7] BiFeO$_3$ NPs,[8] polymer-coated CeO$_2$ NPs,[9] Au NPs,[10] V$_2$O$_5$ nanowires,[11] and FeS sheet[12] had been developed for the assay of H$_2$O$_2$. However, there are major drawbacks for the current colorimetric detection of H$_2$O$_2$ by using either natural enzymes or nanomaterials: (1) The need of peroxidase substrate as the chromogenic reagent in acidic condition (i.e., 3,3,5,5-tetramethylbenzidine (TMB) at pH 4.0) renders all the available assay of H$_2$O$_2$ to be performed in an indirect way. (2) The incubation time of the coloration based on the nanomaterials is in a range of minutes. Therefore, new technology or materials are needed to achieve rapid, direct and facile assay of H$_2$O$_2$.

Because of high chemical and physical stability in ambient conditions, easy preparation, low fabrication cost, nontoxicity, excellent biocompatibility, and environmental friendliness, TiO$_2$ has been widely used in energy and environmental science and technologies, such as photocatalysis, self-cleaning, solar cells, etc.[13−18] Zuo and co-workers have shown that the Ti^{3+}-doped TiO$_2$ (i.e., self-doped titania) can enhance the performance of hydrogen generation.[19] This implies that the presence of Ti^{3+} may transform TiO$_2$ as a reducing agent to directly assay H$_2$O$_2$. Here, we reported a one-step method to prepare heavily Ti^{3+} self-doped TiO$_2$ NPs (herein after, TiO$_2$:Ti^{3+} NPs), which unexpectedly possess rapid and high sensitivity for determining H$_2$O$_2$ without using any peroxidase substrate. The coloration response is instantaneous (<1 s), the sensitive concentration range is as large as 1×10^{-6} to 1 M, and

the detection limitation can reach to 5×10^{-7} M, even lower than that of the HRP.

2. RESULTS AND DISCUSSION

TiO_2:Ti^{3+} NPs were fabricated by ablating rutile TiO_2 powder dispersed in deionized water (concentration: 10 mg/mL) via a 355 nm nanosecond pulsed Nd:YAG laser (6 ns, 10 Hz, typical laser fluence: ~1 J/(pulse cm^2)). Blue color was instantly appeared in the white emulsion containing TiO_2 powders after 355 nm laser irradiation for ~1 min. The emulsion eventually became transparent with blue color after ~10 min of irradiation.

The calculated laser fluence for anatase TiO_2 to heat an individual spherical particle (diameter: 60 nm) to full melting is ~0.6 J/(pulse cm^2).[20] The rutile TiO_2 has similar physical parameters with anatase; we assume the laser fluence threshold is same to that of anatase. The 355 nm Nd:YAG laser fluence used in this study is about ~1 J/pulse·cm^2, which is high enough to fully melt the TiO_2 nanoparticles. During the ablation process, TiO_2 nanoparticles were generated by heat evaporation arisen from the absorption of laser light.[20,21] After 10 min of irradiation, a blue and transparent solution without any precipitate was obtained. The zeta potential of the TiO_2 nanoparticles colloide solution is about −59 mV. The as-prepared TiO_2 NPs is spherelike with average size of about 30 nm, as shown in Figure 1c. According to the electron
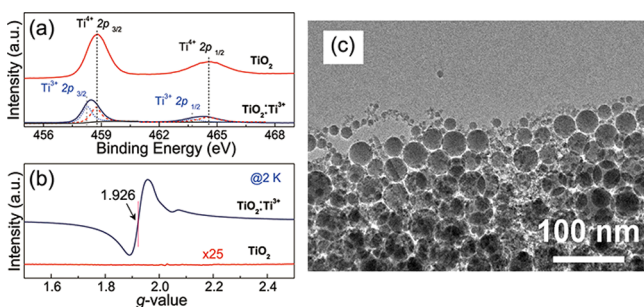
Figure 1. (a) Ti 2p XPS spectra and (b) EPR spectra at 2 K for rutile TiO_2 before and after 355 nm laser irradiation; (c) TEM of TiO_2:Ti^{3+} NPs.

diffraction, the TiO_2:Ti^{3+} NPs is amorphous, as shown in Figure S1 in the Supporting Information. The atomic percentage of O and Ti determined from energy-dispersive X-ray spectrometer (EDX) is 67.84 and 32.16%, respectively. These values are consistent with the atomic constitution of TiO_2, as shown in Figure S1b in the Supporting Information. It is noted that the solution is stable in ambient conditions for more than 3 months without any evident color variation or deposit formation.

The high resolution Ti 2p X-ray photoelectron spectra (XPS) of the TiO_2 powders before and after laser irradiation are shown in Figure 1a. For the pristine TiO_2, the binding energy peaks at 458.9 and 464.7 eV are assigned to the $2p_{3/2}$ and $2p_{1/2}$ core levels of Ti^{4+}. After laser irradiation, the $2p_{3/2}$ and $2p_{1/2}$ peaks shift to a lower energy side. The fitting of the Ti $2p_{1/2}$ peak reveals the presence of two peak energies at 463.7 and 464.5 eV. The Ti $2p_{3/2}$ peak can also be resolved into two Gaussian peaks with peak energy at 458.2 and 458.7 eV. The binding energy of 458.2 and 462.5 eV can attribute to the $2p_{1/2}$ and $2p_{3/2}$ core level of Ti^{3+} respectively. On the other hand, the peak energies at 458.7 and 463.7 eV are related to the $2p_{1/2}$ and

$2p_{3/2}$ core level of Ti^{4+} respectively. These resolutions of peaks are well consistent with the recently reported on the binding energy value of TiO_2 nanostructures containing Ti^{3+} synthesized by chemical method.[22,23] These quantitatively analysis of the XPS data indicates that the Ti^{3+}/(Ti^{3+}+Ti^{4+}) atomic ratio is about 49%, i.e., nearly half of the titanium species in TiO_2:Ti^{3+} are presented in the form of Ti^{3+}. The existence of Ti^{3+} can also be verified by the EPR spectrum, as shown in Figure 1b. The dried TiO_2:Ti^{3+} blue powder gives rise to a very strong electron paramagnetic resonance (EPR) signal, while no evident signal is seen for the pristine rutile TiO_2 powder. The g-value signal can be attributed to originate from the surface and subsurface paramagnetic Ti^{3+} centers, which has also been previouly reported in Ti^{3+}-doped TiO_2 grown by chemcial method.[24−26]

The blue coloration was also reported previously in the reduced TiO_2 (TiO_{2-x}),[19,27−30] nonaqueous-synthesized TiO_2 nanocrystals,[24] and raw TiO_2 irradiated by ultraviolet light in an inert atmosphere.[25,31] The observation of blue coloration can be attributed to the Ti^{3+} species formed in TiO_2. In the reduced TiO_2 (TiO_{2-x}), additional electrons (i.e., blue color) are resulted from the titanium interstitials or oxygen vacancies arisen during the synthetic process. In the nonaqueous-synthesized TiO_2 NPs, the blue coloration is stable in air for several months without any noticeable change in the absorbance.[24] For the TiO_2 under ultraviolet light irradiation, bandgap absorption produces conduction band electrons which localize on the surface of Ti atoms, and this coloration can be rapidly extinguished upon exposure to oxygen.[25] In this study, the dried TiO_2:Ti^{3+} blue powder can be stable in air more than 1 month.

Figure 2a shows the typical absorption spectra and photo images of the TiO_2:Ti^{3+} NPs with and without adding H_2O_2.
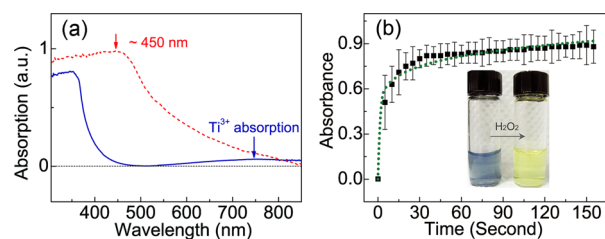
Figure 2. (a) Typical absorption spectra of TiO_2:Ti^{3+} before (solid line) and after (dashed line) adding of H_2O_2. (b) Typical absorbance kinetic of TiO_2:Ti^{3+} NPs and H_2O_2 at 450 nm. Inset shows schematic images of TiO_2:Ti^{3+} NPs without (left) and with (right) adding of H_2O_2 solution. Error bar: standard deviation.

The spectrum of the TiO_2:Ti^{3+} NPs (without H_2O_2) shows a sharp absorption edge at 390 nm (3.18 eV) corresponding to band-to-band transition. As the particle size (~30 nm) is much shorter than the wavelength of visible light (400−800 nm), light scattering caused by the NPs do not contribute to any absorbance in the absorption spectrum. The weak absorption in the visible region may be due to the Ti^{3+}-ion-related level in the band gap.[24] The TiO_2:Ti^{3+} NPs have negligible light absorption over the wavelength between 440 and 530 nm. As shown in Figure 2b, the TiO_2:Ti^{3+} NP solution produces an orange-yellow color after introducing H_2O_2. The solution remained transparent, and there is no deposition formed even adding excessive H_2O_2. The absorbance of the TiO_2 NP-H_2O_2 system in the visible light and near UV ranges is dramatically enhanced when compared to the TiO_2:Ti^{3+} NPs. The resulting solution shows a maximum absorbance at 450 nm, which corresponds to

the orange-yellow color of the systems. It should be pointed out that the blue solution instantly produce orange-yellow color after mixing the TiO_2 NPs with H_2O_2, as shown in the Supporting Information (video).

For H_2O_2 detection based on other nanomaterials, such as V_2O_5,[11] Fe_3O_4,[1,2] and Au,[10] the coloration reaction needs TMB as the peroxidase substrate, the mixture of nanomaterials, TMB substrate and H_2O_2 is generally required to be incubated for some "time interval" in acidic environment at about 45 °C before the corresponding absorption spectra are recongized as a valid measurement.[1,2,4] See Table 1 for the required "time

Table 1. Comparison of Typical Nanomaterials for H_2O_2 Detection

nanomaterials	chromogenic peroxidase substrates[a]	incubation time (s)	pH	detection limit (μM)
V_2O_5 nanowires[11]	ABTS, TMB	60	4.0	
PtPd-Fe_3O_4 nanoparticles[2]	TMB	300	5.2	2
Fe_3O_4 nanoparticles[5]	DAB, OPD	600	3.5	
Au nanoparticles[10]	TMB	600	4.0	0.5
graphene oxide[7]	TMB		4.0	0.05
Ti^{3+}-doped TiO_2	none	none	7.0	0.5

[a]ABTS, 2,2-azino-bis(3-ethylbenzothiazoline-6-sulfonic acid; TMB, 3,3,5,5,-tetramethyl-benzidine; DAB, diazo-aminobenzene; OPD, o-phenylenediamine.

interval" for different types of nanomaterials for the detection of H_2O_2. In our case, no chemical is added to the mixture TiO_2:Ti^{3+} NPs and H_2O_2 so that incubation process is not required to detect H_2O_2 and the "time interval" is zero. Figure 2b illustrates the variation of absorbance at wavelength of 450 nm with time after the TiO_2:Ti^{3+} NPs and H_2O_2 were mixed together. The absorbance at ~450 nm quickly increases with time and becomes stable after ~30 s.

It was reported that similar yellow color solution was also produced in the hydrogen peroxide solution treated with titanium(IV) sulfate reagent with the presence of dilute sulphuric acid[32] or gray TiH_2 powders.[33] The yellow species were tentatively attributed to the formation of pertitanic acid H_2TiO_4.[32] The elemental analysis obtained from the EDX in TEM shows that the atomic ratio of O to Ti is about 4.8/1, which is close to the Ti and O elemental constitution in H_2TiO_4. See also the measured data of H_2TiO_4 given in the Supporting Information. Hence, a possible chemical reaction is tentatively proposed below to explain the reaction between TiO_2:Ti^{3+} NPs and H_2O_2:[34,35]

$$\underset{\text{blue}}{Ti^{3+}} + H_2O_2 + 2H_2O \rightarrow \underset{\text{yellow}}{H_2TiO_4} + 3H^+$$
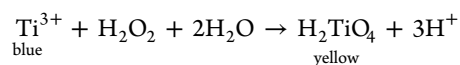
The presence of Ti^{3+} ions and high surface-to-volume area of NPs greatly enhance the reducibility of TiO_2:Ti^{3+} NPs, and can be directly oxidized by H_2O_2. As a result, the Ti^{3+} ions in TiO_2:Ti^{3+} NPs can directly react with H_2O_2, and the resultant pertitanic acid is orange-yellow. Furthermore, the small size NPs with high surface-to-volume ratio accelerate the above chemical reaction. The pertitanic acid can be written as $TiO_2 \cdot H_2O_2$, showing a true peroxide structure. As a comparison, the precursor of white rutile TiO_2 powders without Ti^{3+} ions was also treated with H_2O_2 solution, however, there is no evident

change of color, as shown in Figure S3 in the Supporting Information.

To investigate the reduction capability of H_2O_2 by TiO_2:Ti^{3+} NPs, H_2O_2 with different concentration was added to the TiO_2:Ti^{3+} NPs solution with concentration of 10 mg/mL, as shown in Figure 3 and Figure S6 in the Supporting
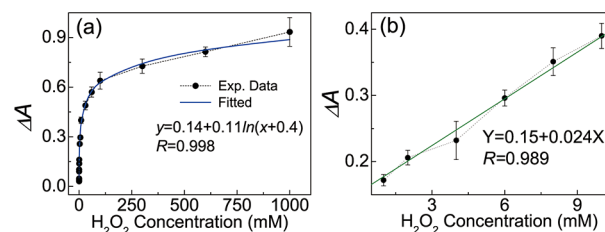
Figure 3. (a) Relationship between absolute absorbance ΔA at 450 nm and concentration of H_2O_2 over a range between 1×10^{-6} and 1 M. The blue solid line is the fitted curve. (b) Linear fiting of absolute absorbance at 450 nm versus H_2O_2 concentration over a range between 1 and 10 mM. Error bar: standard deviation.

Information. The absorbance at 450 nm was selected as the calibration wavelength. The absolute absorbance ΔA is defined as $\Delta A = A(TiO_2-H_2O_2) - A(TiO_2)$, where $A(TiO_2-H_2O_2)$ and $A(TiO_2)$ are the absorbance at 450 nm of TiO_2:Ti^{3+} NP-H_2O_2 system and the corresponding TiO_2:Ti^{3+} NPs solution with same concentration respectively. The ΔA of the system $(TiO_2-H_2O_2)$ increases with the increase of H_2O_2 concentration. As shown in Figure 3a, the absorbance at 450 nm versus H_2O_2 concentration can be well fitted by logarithmic function (with the R value is equal to 0.998) over a wide range of H_2O_2 concentration between 1×10^{-6} and 6×10^{-5} M as well as 1×10^{-4} and 1 M. The detection limit is as low as 5×10^{-7} M. In a small concentration range of 1 mM to 10 mM, the ΔA has a linear relationship ($R = 0.989$) with H_2O_2 concentration.

HCl, NaClO, ethanol, and acetone were selected as the control reagents to verify the coloration of TiO_2:Ti^{3+} NPs solution. The blue transparent solutions became muddy white after adding with HCl and NaClO. This observation is different to that from adding H_2O_2 to the TiO_2:Ti^{3+} NPs solution (i.e., formation of orange-yellow transparent solution; see the inset of Figure 4, the absorption spectra are shown in Figure S5 in the Supporting Information). On the other hand, the adding of ethanol and acetone has shown no evidence of changing in TiO_2:Ti^{3+} NPs solution except the blue color turn light. The absorbance of TiO_2:Ti^{3+} NPs solution with H_2O_2 is much
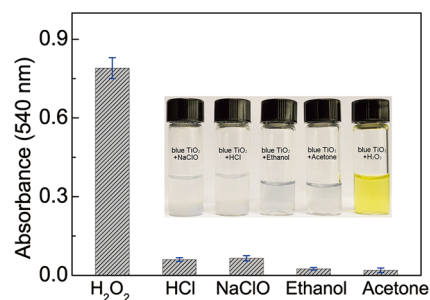
Figure 4. Selectivity analysis for H_2O_2 detection by monitoring the relative absorbance. Inset: the analyte concentrations are as follows: 1 M sodium hypochlorite (NaClO), 2 M hydrochloric acid (HCl), 1 M ethanol, 1 M acetone, 0.5 M hydrogen peroxide (H_2O_2). Error bar: standard deviation.

higher than that with HCl, NaClO, ethanol, and acetone, as shown in Figure 4. This control experiment indicates that the TiO_2:Ti^{3+} NPs shows high selectivity in detection of H_2O_2.

3. CONCLUSIONS

In conclusion, we reported that the fabrication of TiO_2:Ti^{3+} composed of uniform nanospheres grown by a one-step method. The TiO_2:Ti^{3+} NPs exhibit excellent detection behavior of H_2O_2 with high selectivity and required the usage of no peroxidase substrate, such as TMB. Due to free of incubation process, the response time of H_2O_2 detection based on TiO_2:Ti^{3+}NPs is much faster than currently used materials. Detection sensitivity of TiO_2:Ti^{3+}NPs on H_2O_2 is ranged from 1×10^{-6} to 1 M with a detection limit at 5×10^{-7} M. The results demonstrate that the TiO_2:Ti^{3+} NPs can act as an direct, ultrafast H_2O_2 detection agent. Due to easy preparation, low cost, nontoxicity, excellent biocompatibility and environmentally friendly of TiO_2, our findings open up a wide range of new potential applications for TiO_2 NPs in environmental chemistry, biotechnology, pharmaceutical industry, food production.

■ METHODS

1. Fabrication. Typically, 50 mg of commercial available rutile TiO_2 particles (Aladdin Industrial Corporation, 99.8%, with average diameter ∼60 nm) was poured into a glass bottle containing 5 mL of DI water, and the mixture was stirred for 5 min. A pulsed operation (Nd:YAG, 6 ns, 10 Hz) laser beam, which has a wavelength of 355 nm, a beam diameter of ∼5 mm, and laser energy fluence of 1 J/(pulse cm^2), was irradiated onto the mixture of TiO_2 and water. After 10 min of irradiation, the color of mixture becomes dark blue.

2. Characterization. Morphology of the as-prepared TiO_2:Ti^{3+} NPs was investigated by using a JEM-2010 transmission electron microscope (TEM) with accelerating voltage of 200 kV. All the UV−vis absorption and kinetic spectrum was recorded by SHIMADZU UV-2550 spectrometer. The structure of rutile TiO_2 before and after laser irradiation was measured by HORIBA HR-800 Raman system with an argon ion laser (emitted at 488 nm) operating at a back scattering configuration. X-ray photoelectron spectroscopy (XPS) (Kratos AXIS Ultra DLD, Al Kα) was used to determine the chemical compositions of the films with calibration of C 1s peak (284.6 eV). Electron paramagnetic resonance (EPR) spectroscopy (Bruker EMX-10/12 plus) was used to examine paramagnetic species on TiO_2.

3. H_2O_2 Detection Using the TiO_2:Ti^{3+} NPs. A typical colorimetric analysis can be realized as follows: 0.03 mL of H_2O_2 with different concentrations was added into 0.27 mL of 0.4 mM TiO_2:Ti^{3+} NPs solution. The mixture solution becomes orange-yellow color instantly and holds on for 1 min. After the reaction take place for 60 s, the resulting solution was used for absorption spectroscopy measurement. Each data point was repeatly measured for five times to obtain the standard deviation.

■ ASSOCIATED CONTENT

Ⓢ Supporting Information
Transimission elelctron microscopy (TEM), electron diffraction and energy dispersion energy-dispersive X-ray spectroscopy (EDX), Raman spectra of TiO_2:Ti^{3+}. Scanning electron microscopy and Raman spectra of raw rutile TiO_2 nanoparticle.

Photos and the corresponding absorbance at 450 nm of TiO_2:Ti^{3+}, raw rutile TiO_2 after adding H_2O_2; absorption spectrum of TiO_2:Ti^{3+} NPs solution after adding NaClO, HCl, ethanol, and acetone. Images of TiO_2:Ti^{3+} solution with different H_2O_2 concentration. Linear respone of absorbance at 450 nm and H_2O_2 concentration in a narrow range of 1×10^{-3} to 0.06 mM. The live video of the TiO_2:Ti^{3+} colloidal solution mixing with H_2O_2. This material is available free of charge via the Internet at http://pubs.acs.org.

■ AUTHOR INFORMATION

Corresponding Authors
*E-mail: sfyu21@hotmail.com.
*E-mail: sspan@issp.ac.cn

Notes
The authors declare no competing financial interest.

■ REFERENCES

(1) Jiang, Y.; Wang, W.; Li, X.; Wang, X.; Zhou, J.; Mu, X. *ACS Appl. Mater. Interfaces* **2013**, *5*, 1913−1916.
(2) Sun, X. L.; Guo, S. J.; Chung, C. S.; Zhu, W. L.; Sun, S. H. *Adv. Mater.* **2013**, *25*, 132−136.
(3) Kim, M. I.; Shim, J.; Li, T.; Lee, J.; Park, H. G. *Chem.—Eur. J.* **2011**, *17*, 10700−10707.
(4) Tian, J.; Liu, S.; Luo, Y.; Sun, X. *Catal. Sci. Technol.* **2012**, *2*, 432−436.
(5) Gao, L.; Zhuang, J.; Nie, L.; Zhang, J.; Zhang, Y.; Gu, N.; Wang, T.; Feng, J.; Yang, D.; Perrett, S.; Yan, X. *Nat. Nanotechnol.* **2007**, *2*, 577−583.
(6) Song, Y.; Wang, X.; Zhao, C.; Qu, K.; Ren, J.; Qu, X. *Chem.—Eur. J.* **2010**, *16*, 3617−3621.
(7) Song, Y.; Qu, K.; Zhao, C.; Ren, J.; Qu, X. *Adv. Mater.* **2010**, *22*, 2206−2210.
(8) Luo, W.; Li, Y.-S.; Yuan, J.; Zhu, L.; Liu, Z.; Tang, H.; Liu, S. *Talanta* **2010**, *81*, 901−907.
(9) Asati, A.; Santra, S.; Kaittanis, C.; Nath, S.; Perez, J. M. *Angew. Chem., Int. Ed. Engl.* **2009**, *48*, 2308−2312.
(10) Jv, Y.; Li, B.; Cao, R. *Chem. Commun. (Cambridge, U. K.)* **2010**, *46*, 8017−8019.
(11) Andre, R.; Natalio, F.; Humanes, M.; Leppin, J.; Heinze, K.; Wever, R.; Schroeder, H. C.; Mueller, W. E. G.; Tremel, W. *Adv. Funct. Mater.* **2011**, *21*, 501−509.
(12) Dai, Z.; Liu, S.; Bao, J.; Jui, H. *Chem.—Eur. J.* **2009**, *15*, 4321−4326.
(13) Fujishima, A.; Honda, K. *Nature* **1972**, *238*, 37−38.
(14) Oregan, B.; Gratzel, M. *Nature* **1991**, *353*, 737−740.
(15) Asahi, R.; Morikawa, T.; Ohwaki, T.; Aoki, K.; Taga, Y. *Science* **2001**, *293*, 269−271.
(16) Hashimoto, K.; Irie, H.; Fujishima, A. *Jpn. J. Appl. Phys., Part 1* **2005**, *44*, 8269−8285.
(17) Wang, R.; Hashimoto, K.; Fujishima, A.; Chikuni, M.; Kojima, E.; Kitamura, A.; Shimohigoshi, M.; Watanabe, T. *Nature* **1997**, *388*, 431−432.

(18) Miyauchi, M.; Nakajima, A.; Watanabe, T.; Hashimoto, K. *Chem. Mater.* **2002**, *14*, 2812−2816.

(19) Zuo, F.; Wang, L.; Wu, T.; Zhang, Z. Y.; Borchardt, D.; Feng, P. Y. *J. Am. Chem. Soc.* **2010**, *132*, 11856−11857.

(20) Wang, H.; Miyauchi, M.; Ishikawa, Y.; Pyatenko, A.; Koshizaki, N.; Li, Y.; Li, L.; Li, X.; Bando, Y.; Golberg, D. *J. Am. Chem. Soc.* **2011**, *133*, 19102−19109.

(21) Yang, J.; Ling, T.; Wu, W.-T.; Liu, H.; Gao, M.-R.; Ling, C.; Li, L.; Du, X.-W. *Nat Commun* **2013**, *4*, 1695.

(22) Su, J.; Zou, X.-X.; Zou, Y.-C.; Li, G.-D.; Wang, P.-P.; Chen, J.-S. *Inorg. Chem.* **2013**, *52*, 5924−5930.

(23) Zhang, X. B.; Tian, H. M.; Wang, X. Y.; Xue, G. G.; Tian, Z. P.; Zhang, J. Y.; Yuan, S. K.; Yu, T.; Zou, Z. G. *Mater. Lett.* **2013**, *100*, 51−53.

(24) Gordon, T. R.; Cargnello, M.; Paik, T.; Mangolini, F.; Weber, R. T.; Fornasiero, P.; Murray, C. B. *J. Am. Chem. Soc.* **2012**, *134*, 6751−6761.

(25) Howe, R. F.; Gratzel, M. *J. Phys. Chem.* **1985**, *89*, 4495−4499.

(26) Livraghi, S.; Chiesa, M.; Paganini, M. C.; Giamello, E. *J. Phys. Chem. C* **2011**, *115*, 25413−25421.

(27) Teleki, A.; Pratsinis, S. E. *Phys. Chem. Chem. Phys.* **2009**, *11*, 3742−3747.

(28) Liu, G.; Yang, H. G.; Wang, X.; Cheng, L.; Lu, H.; Wang, L.; Lu, G. Q.; Cheng, H.-M. *J. Phys. Chem. C* **2009**, *113*, 21784−21788.

(29) Liu, H.; Ma, H. T.; Li, X. Z.; Li, W. Z.; Wu, M.; Bao, X. H. *Chemosphere* **2003**, *50*, 39−46.

(30) Khomenko, V. M.; Langer, K.; Rager, H.; Fett, A. *Phys. Chem. Miner.* **1998**, *25*, 338−346.

(31) Torimoto, T.; Fox, R. J.; Fox, M. A. *J. Electrochem. Soc.* **1996**, *143*, 3712−3717.

(32) Eisenberg, G. *Ind. Eng. Chem.* **1943**, *15*, 327−328.

(33) Grabstanowicz, L. R.; Gao, S.; Li, T.; Rickard, R. M.; Rajh, T.; Liu, D.-J.; Xu, T. *Inorg. Chem.* **2013**, *52*, 3884−3890.

(34) Rehman, F.; Abdul Majeed, W. S.; Zimmerman, W. B. *Energy Fuels* **2013**, *27*, 2748−2761.

(35) Jin, X.; Wang, X.; Wang, Y.; Ren, H. *Ind. Eng. Chem. Res.* **2013**, *52*, 9726−9730.